AFDEX
Adviser for metal Forming process Design EXpert
Newsletter
Q3 / 2025

MFRC
Metal Forming Research Corporation
www.afdex.com, mfrc@afdex.com
Tel: +82-55-755-7529, Fax: +82-55-761-7529

Contents

1. Upcoming Release: AFDEX V26R01

AFDEX V24R02 was released in May 2025, and the Altair APA version followed this June. These updates were covered in the Q1-Q2 2025 newsletters. AFDEX V26R01 is scheduled for release near the end of 2025, incorporating new features and improvements based on user feedbacks collected throughout the second half of the year.

2. AFDEX Simulation Cases

2.1 Flow curve and Friction

Most academic papers emphasize that the results of metal forming simulations heavily depend on the flow curve and friction conditions. However, especially in cold forming, it is difficult to obtain flow stress data at high strains, such as beyond the fracture point in tensile tests. Using AFDEX MAT, as shown in Figure 2.1, a flow curve up to an effective strain of 0.7 can be obtained from a tensile test on A6061 alloy. This material exhibits low strain hardening, allowing the acquisition of flow stress up to relatively high strains. Beyond that, extrapolation based on the slope of the curve near the limit strain is required, and in cold forging, effective strains beyond this limit frequently occur in major plastic deformation zones.

Friction is an even more complex issue. Many studies commonly emphasize that friction is significantly influenced by pressure, temperature, velocity, real contact area ratio, surface expansion rate, relative speed, material properties, lubricant type and condition, among others. Nevertheless, simplified friction laws based on constant friction coefficients or friction factors are still commonly used.

Notably, many studies rely on constant shear friction law. Wilson [W.R.D. Wilson, Friction and lubrication in bulk metal-forming processes, J. Applied Metalworking 1, 7–19 (1978)] critically reviewed this practice, attributing it to misconceptions formed during early education, particularly in relation to thread tightening in solid mechanics, which is fundamentally different from friction in metal forming.

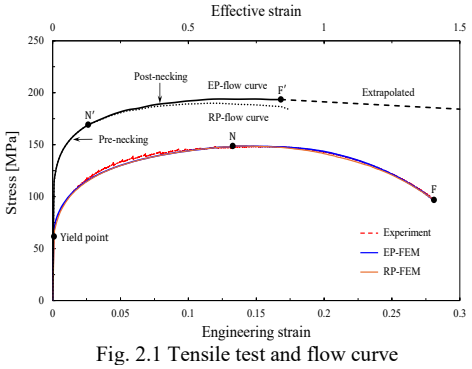

Fig. 2.1 Tensile test and flow curve

In cases involving materials with low strain hardening such as aluminum or ESW materials, friction significantly affects the process. This effect is amplified when the thickness of the workpiece varies by position or when the geometry is strongly influenced by material flow direction, such as in forward-backward extrusion. Additional complexity arises from the strong interdependence of flow behavior and friction—metal forming can be seen as an intense battleground between the two.

Fortunately, flow behavior can be accurately extracted from tensile tests where friction is not involved, albeit within a limited strain range. By applying inverse analysis methods, it is possible to identify appropriate friction conditions. Assuming a simple extrapolated function (e.g., line segments) for the flow curve, both friction and material flow behavior can be determined simultaneously through optimal design inverse analysis.

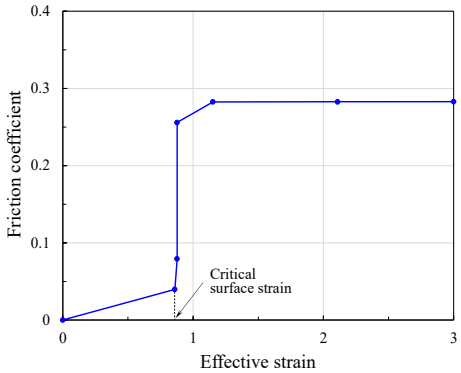

Fig. 2.2 Lubrication regime change

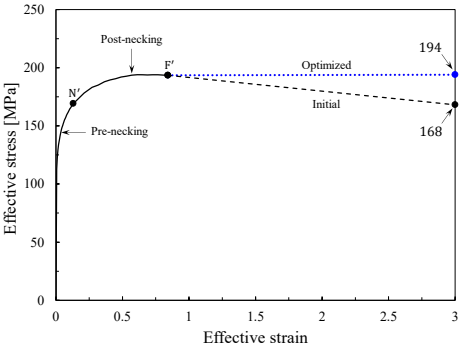

Fig. 2.3 Optimized flow curve

The selected case study involves a type of forward-backward extrusion process where it is particularly difficult to match the target deformation shape. Figures 2.2 and 2.3 show the friction conditions and flow curve, respectively, that yield the best predicted shape. Figure 2.4 compares the experiment and simulation.

Figure 2.2 presents a typical example of a lubrication regime change, where the friction coefficient sharply increases once the surface reaches a specific deformation level. This phenomenon is highly likely to occur during cold or hot forging of low strain-hardening materials such as aluminum.

In Figure 2.3, the optimized flow curve deviates slightly from the simple extrapolated curve (initial flow function used in optimization, shown as a dashed line in Figure 2.1). This deviation likely stems from strain softening behavior that arises near fracture during tensile testing, suggesting that the extrapolated curve might have underestimated flow stress. Nevertheless, the optimized curve remains largely consistent with the pre-fracture flow pattern.

Figure 2.4 compares deformation shapes at two critical locations on the product. It is not possible to accurately predict these shapes using a constant friction coefficient or friction factor. Furthermore, when the initial flow curve (Figure 2.1) is used along with a friction condition optimized under that assumption, the prediction accuracy is lower than when both flow curve and friction are jointly optimized, as in Figure 2.4.

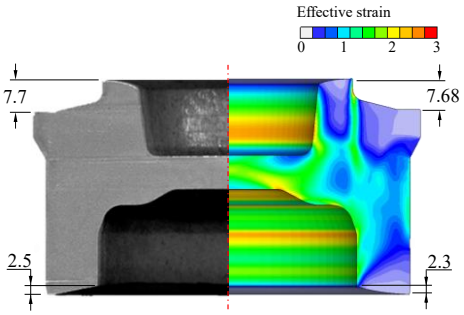

Fig. 2.4 Comparison of experimental and analytical results

2.2 Flow Behavior of Carbon Steel at Room Temperature

S10C, S20C, and S45C carbon steels are commonly used in cold forging. After heat treatment under identical conditions, precise tensile tests were conducted (by TESKO, a NADCAP-certified company). Figure 2.5 shows the test results, and Figure 2.6 presents the flow curves obtained using AFDEX MAT. For this purpose, the flow curve was modeled using a generalized Hollomon model, where the strength coefficient is considered a function of effective strain.

Based on analysis of the tensile test results, the yield strength and the effective strain (true strain) at necking for each material can be expressed as:

$$Y_0(C) = 10.5C^2 + 147.2C + 221.5 \quad (1)$$

$$n_N(C) = -0.346C^2 + 0.039C + 0.204 \quad (2)$$

And the flow curve also has regularity, and the intensity coefficient function can be approximately expressed by the following formula.

$$K(\bar{\varepsilon}) = \begin{cases} K_N, & \bar{\varepsilon} \le n_N \\ \frac{K_{F'} - F_N}{\bar{\varepsilon}_{F'} - n_N}(\bar{\varepsilon} - n_N) + K_n, & n_N < \bar{\varepsilon} \le \varepsilon_{F'} \\ K_{F'}, & \bar{\varepsilon} > \varepsilon_{F'} \end{cases} \quad (3)$$

Where:

$$K_N = -477C^2 + 1100C + 498 \quad (4)$$

$$\bar{\varepsilon}_{F'} = 4.68C^2 - 5.39C + 1.97 \quad (5)$$

$$K_{F'} = -402C^2 + 966C + 562 \quad (6)$$

This set of equations can reproduce the flow curves shown in Figure 2.6 with an average error of less than 0.25%. As illustrated in Figure 2.7, these formulas allow users to generate highly accurate flow functions for any given carbon steel simply by entering the carbon content in AFDEX input data.

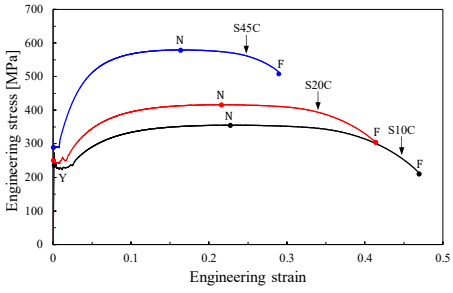

Fig. 2.5 Tensile test results of representative carbon steels

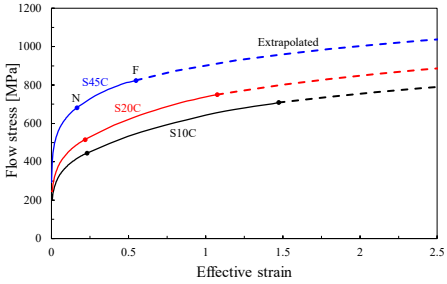

Fig. 2.6 Flow curve

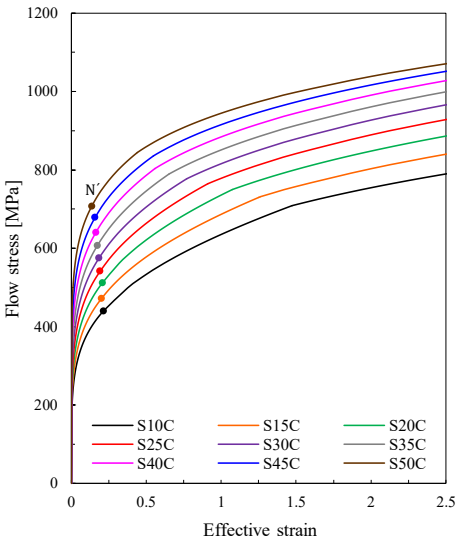

Fig. 2.7 Flow curve of any carbon steel

2.3 Coupling and Casing Pipe Assembly Simulation

Traditional simulation technologies for assembly processes have focused on simple press-fits or threaded joints with relatively few threads. Recently, we analyzed a more complex assembly process involving the coupling and casing pipe, which falls under the category of challenging assembly operations.

The model analyzed was 5.5 inches in size, and the coupling featured approximately 20 threads on one side. The geometry was complex, with about a 1.8° tilt in one direction from the center axis. The simulation focused on a mechanical assembly method in which 16 to 17 threads engaged with each other between the coupling and the casing pipe.

Figures 2.8(a) and 2.8(b) illustrate the simulation model and the initial mesh, respectively. Figures 2.8(c) and 2.8(d) show the distributions of effective strain and stress.

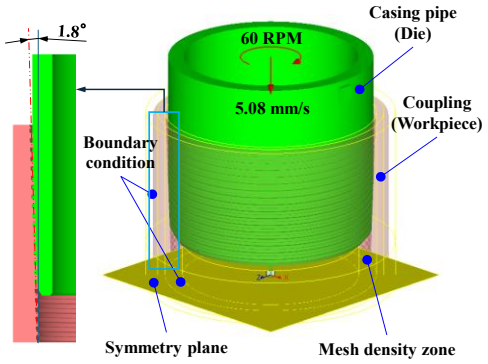

(a) Simulation model

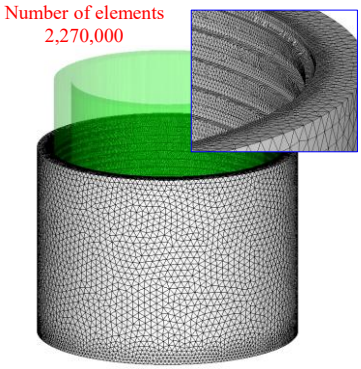

(b) Initial mesh

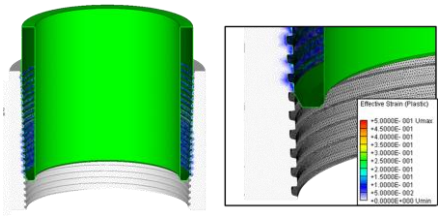

(c) Effective strain distribution

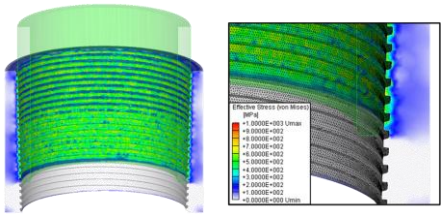

(d) Effective stress distribution

Fig. 2.8 Coupling and Casing Pipe Assembly Simulation

2.4 Flow Forming Process Simulation

Flow forming (including spinning and roll forming) is a metal forming process that shapes a wide variety of product geometries such as sheets, hollow cylinders, and conical shapes using rotating rollers. At the request of a customer, the flow forming simulation was carried out for a virtual cold flow forming process of an automobile wheel rim. Although the target product is formed under cold conditions, real-world flow forming of automobile wheels is also performed under warm and hot conditions, with a wide range of roller shapes and quantities affecting the forming characteristics.

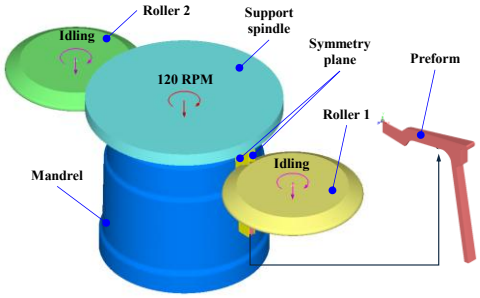

(a) FE simulation model and pre-form shape

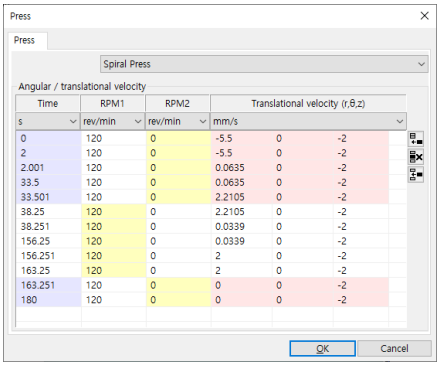

(b) Velocity profile of the rollers over time

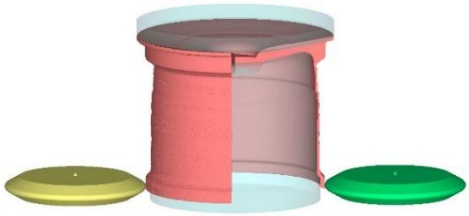

(c) Simulation result

Fig. 2.9 Virtual flow forming simulation of automotive wheel rim

Figure 2.9(a) shows the simulation model. Due to the time-consuming nature of incremental forming (a type of rotary forming), a 10° sector model with symmetry was used to reduce computational cost. Two rollers were employed in the simulation. Figure 2.9(b) presents the roller speed profile over time, and Figure 2.9(c) shows the final simulation result of the virtual flow forming process.

3. AFDEX V26R01

3.1 Enhanced Self-contact Feature

Since AFDEX V24R02, improved routines for self-contact have been implemented. In earlier versions, interference occurred at material interfaces (Figure 3.1(a) center), but the improved version prevents penetration and yields realistic results (Figure 3.1(a) right).

Figure 3.1(b) is the second application example. It is an example where self-contact occurs continuously at the contact surface of the die. The simulation results emphasize that relatively sophisticated self-contact problems are being handled.

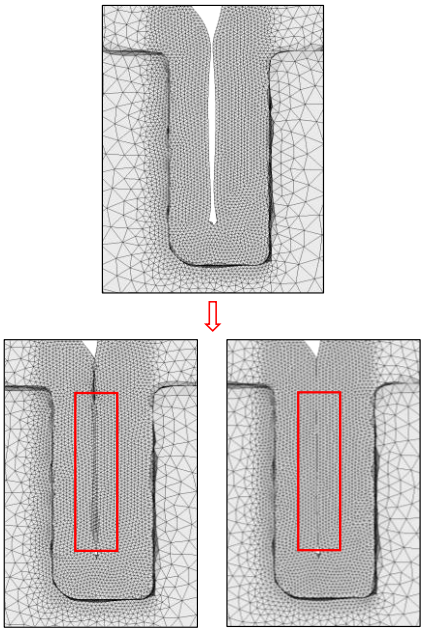

(a)

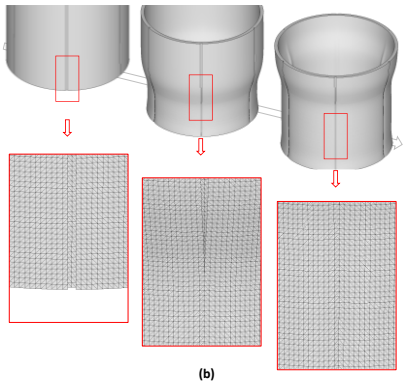

(b)

Fig. 3.1 Continuous self-contact problem

3.2 Expanded 3D Piercing/Trimming Options

In AFDEX 3D, piercing and trimming are performed based on the die to which motion is applied. Users unfamiliar with this functionality often make mistakes when setting up these processes. To support user understanding and minimize errors, explanatory images for this function have been added to the input condition window. Starting with AFDEX V26R01, three selectable options will be available:

1. Perform piercing or trimming immediately without any preforming step
2. Choose whether to remove material projected onto the die with assigned motion
3. Enable automatic extraction of shear zones for piercing and trimming operations

Figure 3.2 shows the updated user interface for piercing and trimming.

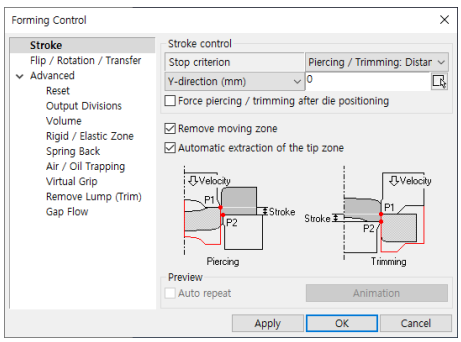

Fig. 3.2 Changed Piercing/Trimming UI

3.3 Improved 2D DXF Import Functionality

Previously, importing CAD files with blocks could cause shape recognition errors. AFDEX V26R01 now supports importing models built with blocks, including those copied or pasted from other files.

3.4 Enhanced Perspective Adjustment in AFDEX SP

By right-clicking on the view background, users can access perspective settings. In prior versions, changing angles automatically altered the distance between camera and focal point, distorting the model size. A new feature locks this distance to maintain appropriate scaling. Figure 3.3 illustrates the perspective setting window and application results.

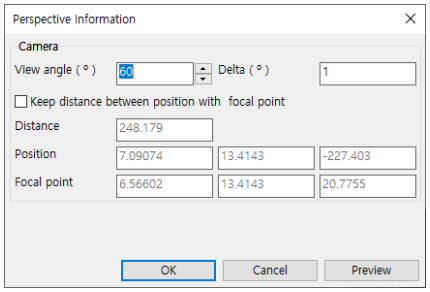

(a) Perspective adjustment settings window

(b) Forged products

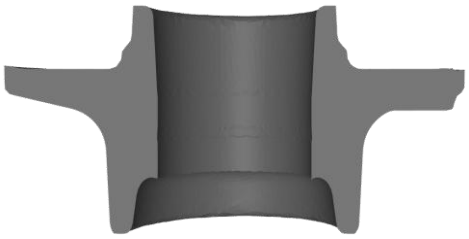

(c) Analysis results with perspective applied

Figure 3.3 Example of applying the perspective adjustment function setting

3.5 Improved License Manager

From AFDEX V24R01, licenses transitioned to a network-based type. However, license manager did not auto-start after server PC reboot. It is now converted to a service app. Since AFDEX V24R02, the license manager is separated for server installation. Client PCs can use licenses by entering the server's IP and port.

4. Notices

4.1 Altair AI+CAE Technology Events

We recently participated in our partner Altair's latest AI+CAE technology events held in APAC regions including Korea, Indonesia, Taiwan, and Japan (Altair Technology Day Indonesia 2025, ATC Taiwan 2025, ATC Japan 2025).

MFRC is also planning to attend the ATC Malaysia 2025 event in Malaysia in July.

(a) Altair Technology Day Indonesia 2025

(b) Altair Technology Conference Taiwan 2025

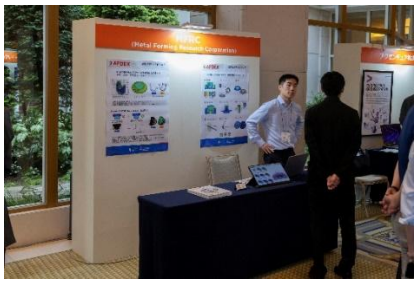

(c) Altair Technology Conference Japan 2025

(d) Altair Technology Conference Malaysia 2025

Fig. 4.1 Altair AI+CAE Technology Event

4.2 MetalForm China 2025

From June 17 to 20, 2025, MFRC was participated in MetalForm China 2025 (中国（上海）国际金属成形展览会2025), the largest metal forming expo in Asia, held in Shanghai, China.